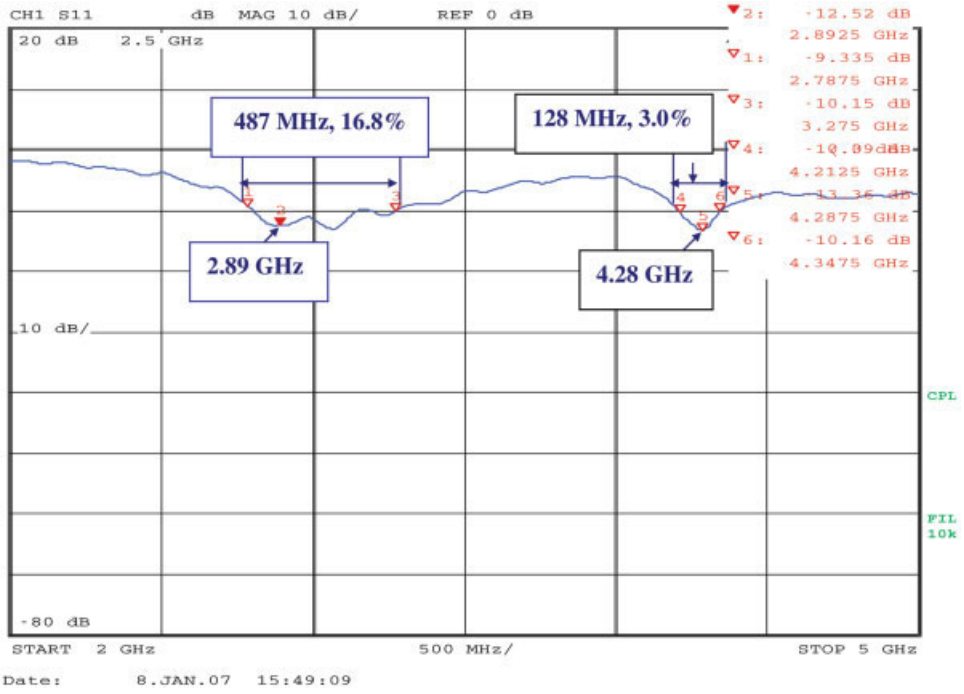

Figure 4 Variation of return loss with frequency for S-MP&SLGPMRMSA-OPMS when $L_{s1} = 14$ mm. [Color figure can be viewed in the online issue, which is available at www.interscience.wiley.com.]

it is seen that there is an enhancement in the bandwidths of f_1 over f_2 and RA. The bandwidth of f_1 is found to be increased by 4.2 times more than the bandwidth of RA. Again this obtained bandwidth of 16.8% is 1.31 times more than single-layer SLRMSA-MSGP. And f_2 has a decrease in the bandwidth when compared with RA.

The lowering of the resonant frequency is due to addition of top patch meandering slits with the meandering slits in the ground plane, which in turn increase the current path length. And the enhancement of the bandwidth is due to stacking configuration.

A measured VSWR for f_1 is 1.602 and f_2 is 1.585 is obtained. The input impedance measured for f_1 is $45.65 + j22.68$ and for f_2 it is $33.45 - j9.239$. Typical coplanar patterns of the antenna at $f_1 = 2.98$ GHz and $f_2 = 4.28$ GHz are measured for both H-plane and E-plane, which are plotted. Good broadside patterns are observed. For $f_1 = 2.905$ GHz, a measured gain of 7.5 dB with $\theta_H = 60°$ and $\theta_E = 62°$ are obtained. For $f_2 = 4.28$ GHz, a measured gain of 3.3 dB with $\theta_H = 120$ and $\theta_E = 70°$ are obtained.

4. CONCLUSIONS

Compact broadband dual-frequency slot-loaded rectangular microstrip antenna with meandering slots in the ground plane and their stacking is presented. By meandering slot-loaded rectangular microstrip antenna with meandering slots in the ground plane, dual frequency compact broadband operation has been achieved. The antenna resonates for dual frequency with a size reduction of 50 and 30% having an enhanced bandwidth of 12 and 4.5%, respectively. Again when a meandered rectangular patch is stacked on the single-layer optimized SLRMSA-MSGP with meandering slits of the top patch in opposite phase with the ground plane meandering slot, the lower resonant frequency is further lowered giving a compactness of 54% and having significantly enhanced bandwidth of 16.8%. These obtained bandwidths are more than conventional microstrip antenna without slots.

REFERENCES

1. S. Dey and R. Mittra, Compact microstrip patch antenna, Microwave Opt Technol Lett 13 (1996), 12-14.
2. K.L. Wong, C.L. Tang, and H.T. Chen, A compact meandered circular microstrip antenna with a shorting pin, Microwave Opt Technol Lett 15 (1997), 147-149.
3. J.H. Lu and K.L. Wong, Slot-loaded, meandered rectangular microstrip antenna with compact dual-frequency operation, Electron Lett 34 (1998), 1048-1050.
4. J.S. Kuo and K.L. Wong, A compact microstrip antenna with meandering slots in the ground plane, Microwave Opt Technol Lett 29 (2001), 95-97.
5. J.I. Bhal and P. Bharatia, Microstrip Antennas, Artech House, Dednam, MA, 1980.
6. D.M. Pozar, Microwave Engineering, Wesley, 1990.
7. K.C. Gupta, Microwaves, Wiley Eastern, New Delhi, 1976.

A NOVELTIME-DOMAIN TECHNIQUE FOR NONPARAXIAL ULTRA SHORT OPTICAL PULSES

Husain M. Masoudi
Electrical and Computer Engineering Department, Emerging Communications Technology Institute, University of Toronto, 10 King's College Road, Ont, Canada M5S 3G4; Corresponding author: husainm@kfupm.edu.sa

Received 10 March 2007

ABSTRACT: *A novel nonparaxial technique based on Pade approximant for modeling ultra short optical pulses has been discussed and verified. The characterization of the technique shows excellent performance in terms of accuracy, efficiency, and stability where the tradi-*

tional paraxial time-domain beam propagation method failed to achieve. The new method is very useful and efficient for modeling long optical pulse interaction when compared to the classical finite-difference time-domain. © 2007 Wiley Periodicals, Inc. Microwave Opt Technol Lett 49: 2481–2486, 2007; Published online in Wiley InterScience (www.interscience.wiley.com). DOI 10.1002/mop.22796

Key words: *non-paraxial equations; Pade approximant; ultra short optical pulse; beam propagation method; modeling; numerical analysis; partial differential equation; finite-difference*

1. INTRODUCTION

Nowadays there are many challenges facing optical engineers to produce efficient and reliable optical communication circuits. Usually, it is not easy to predict the behavior of these devices well in advance and it is natural to resort to modeling techniques to understand and design efficient and novel devices. In modeling direction, there are also many difficulties in predicting today's and future optical circuits. The first challenge is that most of these devices are designed on the bases of pulsed optical beams operation rather than CW. In this context, time-domain (TD) techniques are very essential. The second challenge is that most of these devices are designed for interaction over long optical distances, usually in the order of thousands of wavelengths. Third, modeling techniques have to be efficient and run easily on today's computer resources, otherwise it becomes very monotonous if it requires special computer resources such as supercomputers that very few have access to. The prime technique developed and used over the years for the analysis of time domain problems is the well-known finite-difference time-domain (FDTD) [1-4]. It is understood that the FDTD is suitable for both TD and CW problems, but it requires huge computer resources and more importantly it is not suited for long optical pulse interaction. Propagation techniques such as the beam propagation method (BPM) are well suited for long device interaction [5-7]. However, the known BPM has been mostly developed for CW operation. Over the last few years, there were many progresses to develop new time-domain techniques to undertake these kinds of problems. The majority of these techniques are very similar in their styles to the FDTD approach. In general, there two types of TD methods along this line. The first are called slowly varying methods, in which the first order time derivative is used as a stepping mechanism [8]. Obviously, these are not suited for short optical pulse propagation and can be considered CW methods rather than TD. The second class is similar to the first group in its principle approach, but they use higher order approximation such as Pade relations to account for the neglected second derivative of time [9-11]. It turns out, unfortunately, that most of these techniques consume more computer resources than the FDTD [11]. One way to model long optical devices of TD interaction is to use the BPM principle of one way propagation. A few years back we proposed two efficient paraxial TD-BPM techniques for that purpose [12, 13]. The techniques were very useful for short optical pulse durations, but failed to model ultra short pulses because of the paraxial approximation involved. Recently, a new technique based on the same principle managed to develop a finite-element method to model short pulses [14]. The method uses Pade recurrence approximation after the negligence of a few operator derivatives. In this work we developed a new nonparaxial time-domain BPM based on the same principle of the paraxial TD-BPM given in [12, 13]. First, the TD wave equation was written as a one-way propagational operator and then the recently developed rational complex coefficient approximation of the well known Pade approximant has been used to break the paraxial difficulty [15-18]. The operator has been tested briefly in a quick communication using a simple example [19]. In this work we show and highlight fundamental characterization issues of the technique and test the convergence of essential numerical parameters and also show full detail of accuracy and stability analysis to model ultra short optical pulses. In addition, a comparison with the paraxial TD-BPM technique has been given in detail.

2. THEORY

Starting with the wave equation as

$$\nabla^2\Phi = \frac{n^2}{c_0^2}\frac{\partial^2\Phi}{\partial t^2}, \tag{1}$$

where $n = n(\mathbf{r})$ is the position-dependent refractive index variation, ∇^2 is the spatial Laplacian operator, and c_0 is the wave velocity in free space. If we take out a carrier frequency ω and a propagation coefficient $k = k_o n_o$ in the direction of propagation z from Φ as

$$\Phi = \phi e^{-jkz} e^{j\omega t} + \text{cc}, \tag{2}$$

where $k_0 = \omega/c_0$, n_0 is a reference refractive index, and cc means the complex conjugate of the previous term. Equation (1) now can be written without the carriers in terms of the field ϕ as

$$\frac{\partial^2\phi}{\partial z^2} - 2jk\frac{\partial\phi}{\partial z} + \nabla_\perp^2\phi + (n^2k_0^2 - k^2)\phi - \frac{n^2}{c_0^2}\frac{\partial^2\phi}{\partial t^2} - 2j\frac{n^2}{c_0}k_0\frac{\partial\phi}{\partial t} = 0, \tag{3}$$

where $\nabla_\perp^2$ is the transverse spatial Laplacian operator. Introducing a moving time coordinate $\tau = t - v_g^{-1}z$ with arbitrary v_g. This is necessary because a compact pulse inside a truncated time window will make the pulse vanishes after a certain propagation distance and it requires that the computational window to be adjusted in time at each propagation step. This alteration in fact moves at the group velocity v_g of the pulse envelope. Then Eq. (3) can be written as [12, 13]

$$\frac{\partial^2\phi}{\partial z^2} - 2jk\frac{\partial\phi}{\partial z} + \nabla_\perp^2\phi + (n^2k_0^2 - k^2)\phi - \frac{n^2}{c_0^2}\frac{\partial^2\phi}{\partial t^2} - 2j\frac{n^2}{c_0}k_0\left(\frac{1}{c_0} - \frac{1}{v_g}\right)\frac{\partial\phi}{\partial t} = 0 \tag{4}$$

To arrive to the parabolic TD-BPM technique, one can simply neglect the first term in Eq. (4) that has the second derivative along the direction of propagation z [12, 13]. On the other hand, to derive the wide-angle TD-BPM (broad band) technique, we define the following square root operator Q as

$$Q^2 = \left[\nabla_\perp^2\phi + (n^2k_0^2 - k^2)\phi - \frac{n^2}{c_0^2}\frac{\partial^2\phi}{\partial t^2} - \frac{2jn^2k_0}{c_0}\left(\frac{1}{c_0} - \frac{1}{v_g}\right)\frac{\partial\phi}{\partial t}\right] \div k_0n_0, \tag{5}$$

and write Eq. (4) as a product form as [15]

$$\left\{\frac{\partial}{\partial z} - jk_0n_0 - jk_0n_0Q\right\}\left\{\frac{\partial}{\partial z} - jk_0n_0 + jk_0n_0Q\right\}\phi = 0. \tag{6}$$

For convenience it is easier to transform the square root operator and write it as

$$Q = \sqrt{1 + X}. \tag{7}$$

We notice that the first operator in (6) is for forward propagation of the optical pulse and the second operator is for backward propagation. If we concentrate on forward propagation of the field ϕ, then we can write the formal solution of (6) as

$$\phi(z) = \exp(jk_0n_0z) \times \exp(-jk_0n_0Qz)\phi(0), \tag{8-a}$$

or

$$\phi(z) = \exp(jk_0n_0z) \times \exp(-jk_0n_0\sqrt{1 + X}z)\phi(0). \tag{8-b}$$

It should be understood here that ϕ (0) is the initial field. The square root operator appearing in (8) can be approximated using different techniques such as Taylor or rational approximation. Recently, an interesting Pade approximant has been proposed and tested based on the rational complex coefficient approximation, which can be written as [15-17]

$$\sqrt{1 + X} \approx \prod_{i=1}^{p} \frac{1 + a_i^p X}{1 + b_i^p X}, \tag{9}$$

where a and b are called Pade coefficients with p being the Pade order. For scattering problems, the Pade coefficients must be chosen to be complex to decrease evanescent modes where the associated error can be reduced by rotating the original real axis branch cut through an angle [16, 17]. This approach is comparable of choosing a complex reference wavenumber as given in [18]. We apply the previous technique to model ultra short optical pulse propagation using finite difference approach. The following section shows the characterization of this operator where accuracy and stability analysis of the operator were tested thoroughly. We also compare the results of this technique with the parabolic TD-BPM counterpart method and show the superiority of the new technique in modeling ultra short optical pulses.

3. IMPLEMENTATIONS AND DISCUSSIONS

The previous technique has been implemented and tested to model ultra short optical pulses using different initial conditions. We consider the propagation of a pulsed optical beam with a temporal Gaussian pulse of the form $\phi(\tau) = e\exp(-\tau^2/\sigma_\tau{}^2)$ is assumed as initial condition at $z = 0$ in all simulations, where σ_τ scales the duration of the initial pulse. To describe the performance of the new technique we apply it to model a known pulse propagation that has analytical formulation [12–14, 19, 20]. In the following simulation, we consider the propagation of a pulsed Gaussian beam in a homogenous nondispersive medium, and then the numerical results are compared with analytical results. Following the work in [20] one can find the evolution of a pulsed Gaussian beam in homogenous space by taking the inverse Fourier transform of the product of Ψ and the Fourier transform of the initial pulse, that can be written as

$$\Psi(r,\varphi,z,t) = \frac{1}{2\pi}\int_{-\infty}^{\infty} \Psi(r,\varphi,z,\omega)\tilde{F}(\omega)e^{-i\omega}d\omega, \tag{10}$$

where $\tilde{F}(\omega)$ is the Fourier transform of the initial pulse and $\tilde{\Psi}$ is defined as follows. r and φ are, respectively, the radial and the azimuthal parameters. With an initial spatial Gaussian waist w_0 at $z = 0$, one can use the well-defined frequency-domain representation of a linearly polarized electric field of an azimuthally symmetric Gaussian beam in a homogeneous medium. The evolution of each frequency component of the spectrum of the wavefunction in homogenous space is given in the frequency-domain as [20]

$$\Psi(r,\varphi,z,\omega) = \Psi_0\sqrt{\frac{w_0}{w(z)}}\exp\left\{i[kz - \eta(z)/2] - r^2\left[\frac{1}{w^2(z)} - \frac{ik}{2R(z)}\right]\right\}, \tag{11}$$

where the waist, the radius of curvature, the phase term, and the diffraction length, respectively, are given by

$$w^2(z) = w_0^2\left[1 + \left(\frac{\lambda z}{\pi w_0^2}\right)^2\right] = w_0^2\left(1 + \frac{z^2}{z_0^2}\right),$$

$$R(z) = z\left[1 + \left(\frac{\pi w_0^2}{\lambda z}\right)^2\right] = z\left(1 + \frac{z_0^2}{z^2}\right),$$

$$\eta(z) = \tan^{-1}\left(\frac{\lambda z}{\pi w_0^2}\right) = \tan^{-1}\left(\frac{z}{z_0}\right),$$

$$z_0 = \frac{\pi w_0^2}{\lambda} = \left(\frac{w_0^2}{2c}\right)\omega.$$

The following results assumed a medium of free space and a wavelength of the carrier frequency to be one. The reference refractive index was chosen to be unity. For simplicity and convenience, let us consider the propagation of pulsed optical beams in a homogenous nondispersive medium that has one spatial dimension z and focus on the convergence of crucial numerical parameters of the new operator. During numerical simulation, boundary conditions for the field are necessary in the time domain. Also, it is necessary to compensate for the displacement of the pulse in the time window as the pulse moves forward, due to the motion of the envelope ϕ at the group velocity. There are two methods to use that allow chasing the time window movement. The first is by using the moving time window technique. Simply it is described by setting zero boundary conditions at the edges of the relative time window (coordinate τ) and moving in the absolute time enclosure (coordinate t) with the group velocity of the pulse, such that the relative motion of the pulse in the time window is cancelled. But, in some cases the required group velocity v_g is not known prior to simulation, in which it has to be computed from the propagation simulation process itself. In this case the second technique can be used, which is based on simple periodic boundary conditions. The ends of the relative time window in which that the pulse exiting at one side simply re-enters at the other side of the time window. Both of these techniques were tested numerically and proved to be very useful. It is to be noticed that these techniques are fundamental in terms of saving computer resources. They allow the time window to be of a finite amount multiple of the optical pulse widths.

Figure 1 shows the convergence of the technique with the change of the total time window size T for three different ultra short pulse widths. The errors shown are for the percentage maximum field error, the percentage error of the field at the peak of the

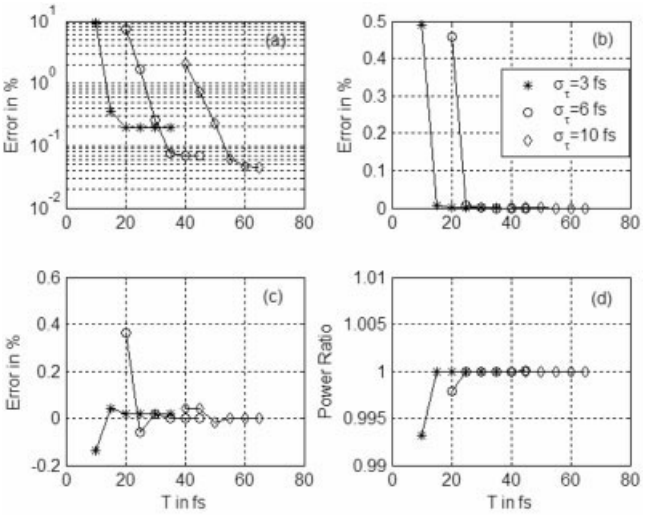

Figure 1 The effect of changing the size of the time window T on the accuracy of the technique for different initial ultra short pulse widths. (a) The percentage maximum field error. (b) The percentage field peak difference. (c) The percentage relative group velocity error. (d) The power ratio of the pulsed beam

pulse, the percentage relative group velocity error of the pulse and the power ratio of the pulsed beam. The pulses were propagated to a distance of $Z = 30$ μm with $p = 6$, $\Delta z = 0.05$ μm, and $\Delta\tau = 0.02$ fs. The purpose behind this experiment is to determine the best and the minimum size of the time numerical window. The figure suggests that the time window T should be at least six times the initial pulse width for optimum results.

Figures 2–4 show the convergence of the technique with the longitudinal step size Δz for different time step sizes and for a Pade order $p = 2$, 4, and 6 respectively. The errors and the power ratio shown have the same definitions of the ones shown in Figure 1. The simulation shown are for an initial pulse width of $\sigma_t = 50$ fs and the pulse was propagated to a distance of $Z = 100$ μm. It is

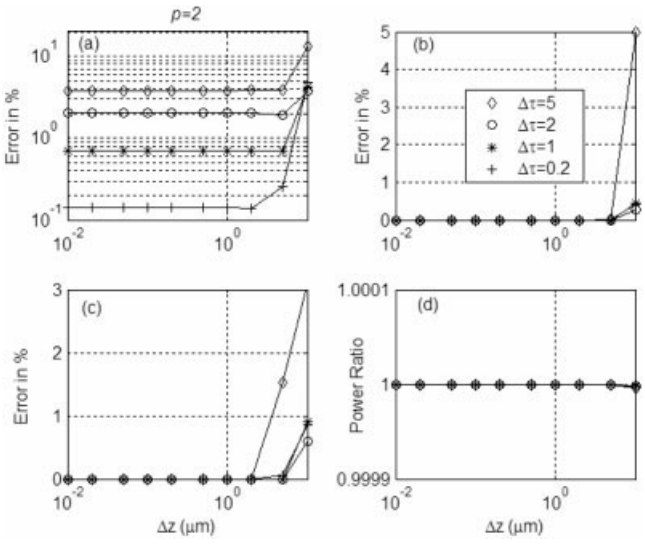

Figure 2 The convergence of the method with the longitudinal step size Δz for different time step sizes and for a Pade order $p = 2$. (a) The percentage maximum field error. (b) The percentage field peak difference. (c) The percentage relative group velocity error. (d) The power ratio of the pulsed beam

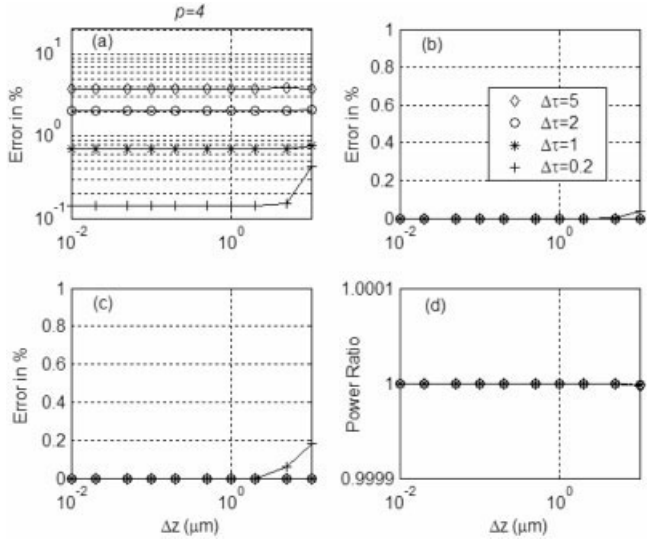

Figure 3 The same as in Figure 2 but for a Pade order $p = 4$

clear from the figures how the convergence of the technique is taking place with as large as of $\Delta z = 10$ μm can be used in some cases. It is to be noticed that the same scale has been kept in these figures for comparison purposes. Also to be noticed from these figures, the remarkable stability of the technique as shown in Figures 2(d), 3(d), and 4(d). Comparison between these results shows that the time step size is the most influential numerical factor that determines the level of the error.

Figure 5 shows a comparison between the present technique and the parabolic method given in [12, 13] for convergence with the longitudinal step size Δz and for different time step sizes. The parameters used in this test are the same parameters used in Figure 4. It is to be noticed that the parabolic method is not stable for values greater than the ones shown in the figure. The field error of the parabolic method changes slightly by the change of the time step size, on the contrary the error of the present technique reduces mostly with the reduction of the time step size. The figure shows the superiority of the present technique over the parabolic counterpart from both error and stability point of views, even though the initial pulse width used is not in the ultra short pulse range.

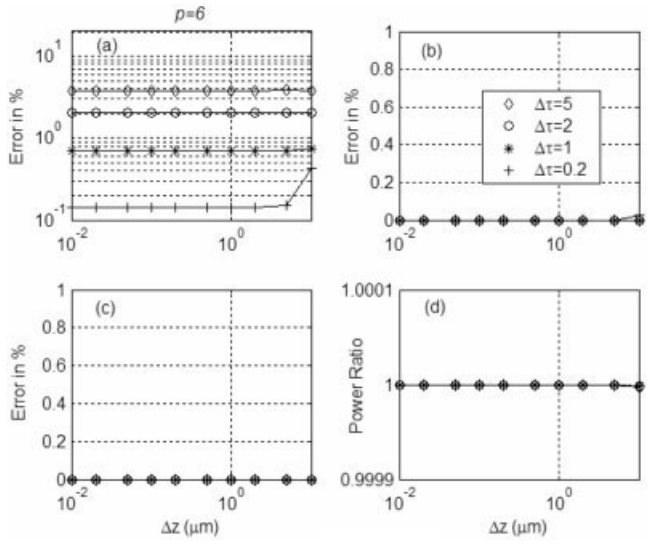

Figure 4 The same as in Figure 2 but for a Pade order $p = 6$

Figure 6 shows a comparison between the present technique and the parabolic method for different initial ultra short pulse widths. The comparison is for different time step sizes and different Pade orders. The parameters used in this test are the same parameters used in Figure 2 with $\Delta z = 0.1$ μm for the wide angle method and for the parabolic method the step sizes were $\Delta z = 0.1$ μm when $\Delta\tau = 1.0$ fs and $\Delta z = 0.0025$ μm when $\Delta\tau = 0.1$ fs. The figure shows the divergence of the parabolic method for ultra short pulse widths even when the time step size is reduced, because the error here is mainly associated with the paraxial approximation. On the other hand, the present technique shows a remarkable performance even for ultra small optical pulse widths. It is to be noticed, as discussed before and as seen in the figure, that the wide angle technique depends mostly on the size of the time step size $\Delta\tau$. This should be understood behavior because in modeling ultra short optical pulses, small time step sizes are needed to represent the rapid variation of the pulse envelope. Again from the figure one also notices the strong stability of the present technique compared with the parabolic counterpart.

4. CONCLUSION

A novel time domain BPM based on Pade approximant has been shown and verified. The technique is for nonparaxial ultra short optical pulse propagation. Detail characterizations of accuracy and stability of the technique have been shown using the propagation of pulsed optical beams in homogenous materials. In addition, full comparison with the limited paraxial TD-BPM counterpart technique has been made. It was concluded that the new technique is very stable, efficient, and accurate in modeling ultra short optical pulse in long propagation interaction.

ACKNOWLEDGMENT

This work was supported by King Fahd University of Petroleum and Minerals KFUPM, Dhahran, Saudi Arabia. The author would like to thank the University of Toronto, Canada for hosting his sabbatical leave with special appreciation to Prof. J. Setwart Aitchison.

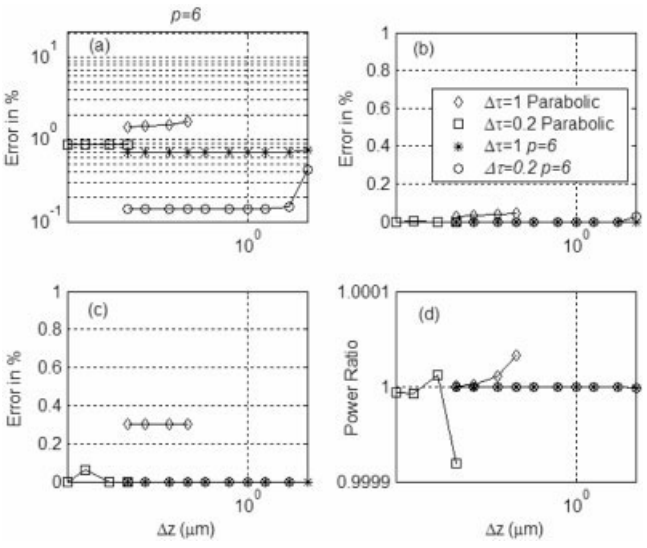

Figure 5 The convergence of the new technique and the parabolic time-domain BPM with the longitudinal step size Δz for different time step sizes and for a Pade order $p = 6$. (a) The percentage maximum field error. (b) The percentage field peak difference. (c) The percentage relative group velocity error. (d) The power ratio of the pulsed beam

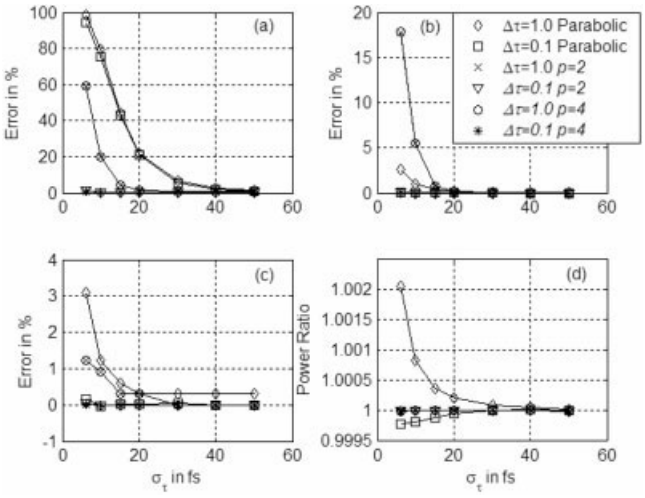

Figure 6 Comparison between the new technique and the parabolic time domain for different initial ultra short pulse width. (a) The percentage maximum field error (b). The percentage field peak difference. (c) The percentage relative group velocity error. (d) The power ratio of the pulsed beam

REFERENCES

1. K.S. Yee, Numerical solution of initial boundary problems involving Maxwell's equations in isotropic media, IEEE Trans Antenna Propag 14 (1966), 302-307.
2. R.W. Ziolkowski, The incorporation of microscopic material models into the FDTD approach for ultrafast optical pulse simulations, IEEE Trans Antenna Propag 45 (1997), 375-391.
3. R.M. Joseph and A. Taflove, FDTD Maxwell's equations models for nonlinear electrodynamics and optics, IEEE Trans Antenna Propag 45 (1997), 364-374.
4. A. Taflove, Review of the formulation and application of the finite-difference time-domain method for numerical modelling of electromagnetic wave infractions with arbitrary structures, Wave Motion 10 (1988), 547-582.
5. M.D. Feit and J.A. Fleck, Light propagation in graded-index optical fibers, App Opt 17 (1978), 3990–3998.
6. D. Yevick, A guide to electric field propagation techniques for guided-wave optics, Opt Quant Electr 26 (1994), 185-197.
7. H.J.W.M. Hoekstra, On beam propagation methods for modelling in integrated optics, Opt Quant Electr 29 (1997), 157-171.
8. F. Ma, Slowly varying envelope simulation of optical waves in time domain with transparent and absorbing boundary conditions, J Lightwave Technol 15 (1997), 1974-1985.
9. J. Shibayama, T. Takahashi, J. Yamauchi, and H. Nakano, Efficient time-domain finite-difference beam propagation methods for the analysis of slab and circular symmetric waveguides, J Lightwave Technol 18 (2000), 437-442.
10. M. Koshiba, Y. Tsuji, and M. Hikari, Time-domain beam propagation method and its application to photonics crystal circuits, J Lightwave Technol 18 (2000), 102-110.
11. J. Shibayama, M. Muraki, J. Yamauchi, and H. Nakano, Comparative study of several time-domain methods for optical waveguide analyses, J Lightwave Technol 23 (2005), 2285-2293.
12. H.M. Masoudi, M.A. AlSunaidi, and J.M. Arnold, Time-domain finite-difference beam propagation method, IEEE Photon Technol Lett 11 (1999), 1274-1276.
13. H.M. Masoudi, M.A. AlSunaidi, and J.M. Arnold, Efficient time-domain beam propagation method for modelling integrated optical devices, J Lightwave Technol 19 (2001), 759-771.
14. L.L. Bravo-Roger, M. Zamboni-Rached, K.Z. Nobrega, et al., Spatio-temporal finite element propagator for ultrashort optical pulses, IEEE Photonics Technol Lett 16 (2004), 132-134.
15. F.A. Milinazzo, C.A. Zala, and G.H. Brooke, Rational square-root

approximations for parabolic equation algorithms, J Acoust Soc Am 101 (1997), 760-766.
16. H. El-Refaei, D. Yevick, and I. Betty, Stable and noniterative bidirectional beam propagation method, IEEE Photonics Technol Lett 12 (2000), 389-391.
17. P.L. Ho and Y.Y. Lu, A stable bidirectional propagation method based on scattering operators, IEEE Photonics Technol Lett 13 (2001), 1316-1318.
18. H. Rao, M.J. Steel, R. Scarmozzino, and R.M. Osgood, Jr., Complex propagators for evanescent waves in bidirectional beam propagation method, J Lightwave Technol 18 (2000), 1155-1160.
19. H.M. Masoudi, A stable time-domain beam propagation method for modelling ultra short optical pulses, in press.
20. R.W. Ziolkowski and J.B. Judkins, Propagation characteristics of ultrawide-bandwidth pulsed Gaussian beams, J Opt Soc Am A 9 (1992), 2021-2030.

NEW AND ACCURATE SYNTHESIS FORMULAS FOR MULTILAYER HOMOGENEOUS COUPLING STRUCTURE

Kerim Guney, Celal Yildiz, Sabri Kaya, and Mustafa Turkmen
Department of Electrical and Electronics Engineering, Faculty of Engineering, Erciyes University, 38039 Kayseri, Turkey;
Corresponding author: kguney@erciyes.edu.tr

Received 13 March 2007

ABSTRACT: *New, accurate closed-form formulas for the synthesis of multilayer homogeneous coupling structure (MHCS) are presented. They are obtained by using a differential evolution algorithm (DEA), and are useful for the computer-aided design (CAD) of MHCS. The average percentage error is found to be 0.38% for 1825 MHCS samples having different electrical parameters and physical dimensions, as compared with the results of the quasi-static analysis.* © 2007 Wiley Periodicals, Inc. Microwave Opt Technol Lett 49: 2486–2489, 2007; Published online in Wiley InterScience (www.interscience.wiley.com). DOI 10.1002/mop.22743

Key words: *multilayer homogeneous coupling structure; synthesis formulas; differential evolution algorithm*

1. INTRODUCTION

Multilayer monolithic microwave integrated circuits (MMICs), which utilize narrow width microstrip lines on thin dielectric materials, have received widespread attention [1–4]. Various small size coupling structures incorporating multilayered dielectrics have been studied in the literature [5–8].

The multilayer homogeneous coupling structure (MHCS) for multilayer MMICs was proposed and analyzed by Gillick et al. [6] in 1993. It offers reduced current crowding at the conductor edges, and is particularly suitable for integration with coplanar waveguide, slot line, and microstrip transmission lines. The closed-form analytical expressions for the characteristic impedances and coupling coefficients of MHCS were derived by using conformal mapping method in [6]. However, to our best knowledge, there is no synthesis formula in the literature to determine the physical dimensions of MHCSs for the required design specifications.

In this article, new and accurate closed-form synthesis formulas obtained by using the differential evolution algorithm (DEA) [9, 10] are proposed to compute easily the physical dimensions of MHCS for odd- and even-mode. Since the DEA is a simple, fast, and robust algorithm, it was used for solving microwave and antenna engineering problems [11–17]. To validate the accuracy of proposed closed-form formulas, the synthesis results obtained in this work are compared with the quasi-static analysis results [6].

2. DIFFERENTIAL EVOLUTION ALGORITHM

DEA, a branch of evolutionary algorithms, has proven to be a highly efficient technique for solving numerical optimization problems [9, 10]. The major benefits of DEA are its simplicity, ease of use, and robustness. Moreover, DEA uses only a few control parameters and these remain fixed throughout the entire optimization procedure.

DEA operates on a population with N_{pop} individuals, or candidate solutions. Each individual of the solution vector is composed N_{par} optimization parameters. To establish a starting point for optimum seeking, the population must be initialized. The initial population is created with random values selected from within the given boundaries:

$$v_{i,j}^{P} = v_j^{\min} + R_j \times (v_j^{\max} - v_j^{\min}), j = 1,2,\cdots,N_{par}, \quad (1)$$

where R_j is a random number, uniformly distributed between 0 and 1, and $v_j^{\min}$ and $v_j^{\max}$ denote the minimum and maximum permissible values of the jth parameter, respectively.

After the initialization, the algorithm goes into genetic evolution, and three genetic operations, namely, mutation, crossover and selection are executed in sequence. The mutation operation is the key procedure in DEA. There are some forms of mutation schemes [9, 10]. In this work, the mutation operation, which generates a mating partner for each individual by producing a difference vector called the mutant vector, is used. The mutant vector can be written as:

$$v^{M,i} = v^{n,\text{opt}} + P_{\text{mut}}(v^{n,p_1} - v^{n,p_2}), i \neq p_1 \text{ and } i \neq p_2, \quad (2)$$

where i, p_1, and p_2 are three randomly selected distinct individual indexes, n is the generation index, P_{mut} is the mutation factor, and the superscripts M and opt refer to the mating pool and the optimal individual in the population, respectively.

Following mutation operation, a trial vector is determined by performing the crossover operation as follows:

$$(v^{C,i})_j = \begin{cases} (v^{M,i})_j, & \gamma \leq P_{\text{cross}} \\ (v^{n,i})_j, & \text{otherwise} \end{cases} \quad (3)$$

where C denotes the population of children, γ is a real random number in the range of [0, 1], and P_{cross} is the probability of a real-valued crossover factor. The trial is then checked, and if an optimization parameter value falls outside the prescribed bounds, it is replaced by a feasible value.

Finally, the selection operation is used to produce better offspring. Each child competes with its parent, and survives only if its fitness value is better. Following this, the next round of genetic evolution then begins. These processes are repeated until a termination criterion is attained or a predetermined generation number is reached.

3. NEW SYNTHESIS FORMULAS FOR MHCS

Figure 1 shows the cross-section of a MHCS where $2H$ is the total thickness of the dielectric material with relative permittivity ε_r, $2S$ is the conductor spacing between the coupled lines, and $2W$ is the gap width in the center ground planes. The placing of coupled